Applied Surface Science 516 (2020) 146129

Contents lists available at ScienceDirect

Applied Surface Science

journal homepage: www.elsevier.com/locate/apsusc

Full Length Article

Outstanding radiation tolerance and mechanical behavior in ultra-fine nanocrystalline $Al_{1.5}CoCrFeNi$ high entropy alloy films under He ion irradiation

Guo Pu[a], Liwei Lin[a], Ran Ang[a], Kun Zhang[a], Bo Liu[c,a,*], Bin Liu[b], Tao Peng[c,*], Shifeng Liu[d], Qiran Li[c,e]

[a] Key Laboratory of Radiation Physics and Technology of Ministry of Education, Institute of Nuclear Science and Technology, Sichuan University, Chengdu 610064, PR China
[b] Powder Metallurgy Research Institute, Central South University, Changsha 410083, PR China
[c] Shenzhen Institutes of Advanced Technology, Chinese Academy of Sciences, Shenzhen 518055, PR China
[d] Xi'an University of Architecture and Technology, Xi' an 710045, PR China
[e] INNOVICES SARL, 1 Place Paul Verlaine, 92100 Boulogne Billancourt, France

ARTICLE INFO

Keywords:
High entropy alloy films
Ultra-fine nano-crystalline
Phase stability
Swelling resistance
Mechanical behavior

ABSTRACT

The enhancement of helium ion (He^+) radiation tolerance and mechanical behavior of high entropy alloys (HEAs) have triggered significant research interest. In this work, the ultra-fine nano-crystalline $Al_{1.5}CoCrFeNi$ HEA films with single phase structure were prepared, which were irradiated at 300 K with 60 keV He^+ in a wide fluence ranging from 1×10^{16} cm^{-2} to 1×10^{17} cm^{-2}. The effects of ultra-fine nano-crystalline on He evolution behavior, radiation tolerance and mechanical behavior in $Al_{1.5}CoCrFeNi$ HEA films were investigated. The results show that the He clusters preferentially distributed along the grain boundaries (GBs) rather than in grains due to the defect sink effect of nano-GBs. No observable He bubbles were observed in the peak damage region of the films even though the He concentration is up to 8.50 at.% at the fluence of 1×10^{17} cm^{-2}. Some grains with limited irradiation damage keep their stability and integrity by eliminating the irradiated defects at GBs, exhibiting enhanced radiation tolerance in the ultra-fine nano-crystalline HEA film. The dependence of phase stability on the suppression of radiation-induced segregation level owing to the design of ultra-fine nano-crystalline and high lattice distortion was revealed in detail. Moreover, the ultra-fine nano-crystalline HEA films display higher swelling resistance than that of bulk coarse-grained HEA materials by reducing the size of He clusters. Higher relative hardness(H/H_0) was observed in the irradiated ultra-fine nano-crystalline HEA film compared to that of the bulk coarse-grained HEA, Finally the relevant hardening mechanisms were also discussed.

1. Introduction

In order to develop a safe, sustainable and efficient nuclear reactor, it is urgent and necessary to seek novel and advanced nuclear reactor's structural materials with superior performance which could be used in the extreme environment of high irradiation damage [1]. Recent decade, high entropy alloys (HEAs) [2,3], based on the concept of concentrated multi-component solid solution, have shown promising properties such as high strength, high ductility, and increased corrosion resistance and so on [2–5]. Some studies have revealed that the HEAs under irradiation conditions demonstrate extraordinary radiation tolerance in mitigating irradiation damages, for example, reduced swelling [6], slower irradiation induced defect migration [7] as well as reduced dislocation size and density [8] in comparison with that of conventional binary or ternary alloys owing to its proposed compositional complexity and high configurational entropy. Therefore, the HEA materials are expected to be a good candidate for future advanced nuclear reactor's structural materials [6–9].

In addition to the investigations of improved radiation tolerance in the coarse-grained HEA bulk materials during ion or electron irradiation [6–10], recent research works have also explored helium (He) evolution behavior after He^+ irradiation, and irradiation induced phase instability after heavy ion or electron irradiation in the coarse-grained HEA bulk materials [11–14]. Generally, the introduced He atoms in

* Corresponding authors.
E-mail addresses: liubo2009@scu.edu.cn (B. Liu), tao.peng@siat.ac.cn (T. Peng).

https://doi.org/10.1016/j.apsusc.2020.146129
Received 11 December 2019; Received in revised form 12 March 2020; Accepted 16 March 2020
Available online 17 March 2020
0169-4332/

coarse grains tend to bind strongly with the vacancies and to further grow into He-clusters or He bubbles, which may cause a series of negative changes in structures and properties, such as voids, dislocation loops, volume swelling and deterioration in mechanical properties. Furthermore, the formation of secondary phase and radiation-induced segregation (RIS) of constituent elements could either be induced or enhanced by the heavy ions and electron irradiation at the defect sinks (dislocation loops, defects clusters and high angle grain boundaries, etc) [14–17]. For instance, the Ni_3Al type phase precipitates in the $Al_{0.12}$CoCrFeNi HEA and $L1_0$ (NiMn)-type ordering decomposition in equiatomic CrFeCoNiMn HEA were both identified due to the RIS at dislocation loops induced by 3 MeV Ni^{2+} and 1.25 MeV electron irradiation [13–14], respectively. M. Barr *et al.* also examined the RIS in the CoCrFeNiMn HEA at high angle grain boundaries under the irradiation damage of 2–3 dpa [17]. The behavior of RIS is known to be a microstructure evolution in the formation of undesirable phases and irradiation assisted stress corrosion cracks in alloys including several conventional Fe-Cr-Ni austenitic alloys [13–14,18]. However, there haven't been any explicit approaches proposing to suppress the irradiation induced phase instability and RIS in the HEAs materials which are exposed to irradiation environment so far. As is well known that the nanocrystallines in materials exhibit additional radiation tolerance compared with the coarse-grained materials due to the high density grain boundaries (GBs), which were regarded as defect sinks since an effective annihilation and reduction of the irradiated defects can be attributed to them [19–20], and also the nano-GBs with three-dimensional network facilitate the solute diffusion uniformity, interstitial/vacancy recombination and inhibit the RIS induced by defect sinks of GB in the alloys [20–22]. It has been reported that the composition precipitation was induced in coarse-grained bulk $Al_{1.5}$CoCrFeNi HEA which was irradiated by 3 MeV Au ions [8]. A great number of research works mainly focused on the investigations of irradiation response of the coarse-grained or the submicron HEA bulks materials including $Al_{1.5}$CoCrFeNi HEA coarse-grained materials. However, so far there was no detailed investigation for the effect of ultra-fine nano-crystallines in HEAs on the He evolution behavior, radiation tolerance and mechanical behavior.

In this study, the ultra-fine nano-crystalline $Al_{1.5}$CoCrFeNi HEA films with single phase structure were obtained by adjusting the radio frequency magnetic sputtering rate (~18.4 nm/min) at room temperature. After that the films were irradiated at 300 K with 60 keV He^+ in a wide fluence ranging from 1×10^{16} cm^{-2} to 1×10^{17} cm^{-2}. The special He distribution behavior and enhanced radiation tolerance in ultra-fine nano-crystalline $Al_{1.5}$CoCrFeNi HEA films was characterized by high resolution transmission electron microscopy (HRTEM). As a contrast, the He morphology and its behavior in coarse-grained $Al_{1.5}$CoCrFeNi HEA bulk materials irradiated at same He^+ fluence were studied by using HRTEM. The different He evolution and formation mechanism were discussed based on the HRTEM results. The dependence of phase stability on the suppression of radiation-induced segregation level owing to the design of ultra-fine nano-crystalline and high lattice distortion was revealed in detail. Besides, the swelling resistance and relative hardness H/H_0 (H: irradiated hardness, H_0: unirradiated hardness) after irradiation were also contrasted between the ultra-fine nano-crystalline $Al_{1.5}$CoCrFeNi HEA films and coarse-grained $Al_{1.5}$CoCrFeNi HEA bulk materials.

2. Experiments

The ultra-fine nano-crystalline $Al_{1.5}$CoCrFeNi HEA films were deposited by RF magnetic sputtering at room temperature on the single-crystalline silicon (Si) substrates, which were ultrasonically cleaned by acetone and alcohol, respectively. The deposition system was evacuated to a background pressure lower than 6×10^{-4} Pa, and then pure Ar with a flow rate of 35 sccm providing the deposition pressure of 0.45 Pa. The composition of $Al_{1.5}$CoCrFeNi target was prepared by powder metallurgy with high purity (99.99%) raw materials of aluminum, cobalt, chromium, iron and nickel powders. The deposition power was controlled at 110 W. The thickness of $Al_{1.5}$CoCrFeNi HEA films is about 450 nm with a deposition time of 24.5 min. During the deposition, the substrates were rotating at a speed of 20 rpm to ensure the uniformity of the films. Additionally, the bulk $Al_{1.5}$CoCrFeNi HEA with average grain size of around 20 μm were prepared by powder metallurgy. Once the samples are ready, they were irradiated with ion fluence ranging from 1×10^{16} cm^{-2} to 1×10^{17} cm^{-2} by 60 keV He^+ irradiation system at room temperature.

Grazing incidence X-ray diffraction (GIXRD) was used to characterize the phase constitution in the films by RigakuDmax 2000 with the Cu Kα radiation, the GIXRD data was recorded at a grazing incidence angle of 2° for the angle scanning range of 20°-80° with a step of 0.01° and a dwell time of 4 s for each step. The displacements per atom (dpa) and the He concentration as a function of depth were calculated by SRIM-2008 with the full cascade TRIM simulation as the $Al_{1.5}$CoCrFeNi HEA is multi-elemental target [23], using the threshold displacement energies of 25 eV for Al atom and of 40 eV for other atoms as well as the HEA density at 6.2449 g/cm^3 [17]. A combination of the High-Resolution Transmission Electron Microscope (HRTEM, Tecnai G^2 F20), Selected Area Electron Diffraction (SAED) and Scanning TEM-Energy Dispersive Spectroscopy (STEM-EDS, FEI F200X Talos) were carried out to characterize the micro-structures of HEA films after He^+ irradiation. The HRTEM foils from the irradiated films were prepared by mechanical polishing, followed by ion milling on a Gatan precision ion polishing system with the final foils thickness of around 100 nm. The micro-structure of $Al_{1.5}$CoCrFeNi HEA bulk materials irradiated at fluence of 1×10^{17} cm^{-2} were also characterized by HRTEM. The induced irradiation swelling and relative hardness H/H_0 were contrasted between the ultra-fine nano-crystalline $Al_{1.5}$CoCrFeNi HEA films and $Al_{1.5}$CoCrFeNi HEA bulk materials. The hardness of $Al_{1.5}$CoCrFeNi HEA films, as well as coarse-grained $Al_{1.5}$CoCrFeNi HEA was investigated by using a MTS nano-indenter with Continuous Stiffness Measurement (CSM) technique in XP mode.

3. Results and discussions

Fig. 1 shows the variation in the GIXRD spectra of the ultra-fine nano-crystalline $Al_{1.5}$CoCrFeNi HEA films before and after irradiation at 300 K. The X-ray diffraction result indicates that the as-deposited film is body centered cubic (BCC) single-phase structure due to the fact that Al atoms molar ratio is increased to 1.5 [24]. It is noteworthy that there is

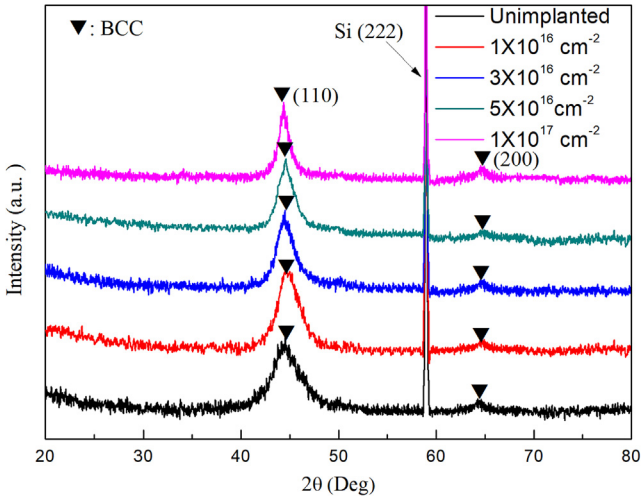

Fig. 1. GIXRD patterns of $Al_{1.5}$CoCrFeNi HEA films before and after He^+ irradiation with fluence ranging from 1×10^{16} cm^{-2} to 1×10^{17} cm^{-2} of 60 keV He^+ in the implantation system.

no variation in phase composition after He^+ irradiation at the fluence ranging from 1×10^{16} cm^{-2} to 1×10^{17} cm^{-2}, indicating that the phase structure keeps stability after He^+ irradiation. The crystalline size was estimated by the Scherrer formula [25] as follow:

$$D = \frac{0.89 \times \lambda}{\beta \times \cos\theta} \quad (1)$$

where λ is the wavelength of Cu Kα radiation, β is the calibrated full-width at half-maximum of a Bragg peak, and θ is the Bragg angle. The crystalline size of the as-deposited film is about 5 nm, and the crystalline sizes of irradiated films are ranging from 5 nm to 7 nm, showing that the ultra-fine nano-crystalline was obtained in the $Al_{1.5}CoCrFeNi$ HEA films by adjusting the RF magnetic sputtering rate (18.4 nm/min) and the crystalline sizes exhibit good stability tolerance after He^+ irradiation, which will be confirmed by the HRTEM results in the subsequent paragraph. The slight reduction of (1 1 0) peak intensity and peak positions shift to lower angle with increasing of He^+ fluences. The reduction of peak intensity is an indication of disordering of crystal lattices due to the irradiated defects. Moreover, the shift of peak position is caused by enlargement of lattice spacing in the direction of which is normal to surface, which will be further identified in the following experimental results.

Fig. 2 shows the SRIM simulation results and HRTEM images for the $Al_{1.5}CoCrFeNi$ HEA film irradiated with 60 keV He^+ at the fluence of 1×10^{17} cm^{-2}. As shown in Fig. 2(a), the calculated maximum values of irradiation damage (the values of DPA) and He concentration are about 8.03 dpa and 8.50 at.%, respectively. According to the curves of SRIM simulation, the peak damage region is roughly located at 200 nm in depth from the surface of samples. Fig. 2(b) shows the cross-section HRTEM image of the slightly damaged subsurface layer of ~120 nm width of HEA film which was irradiated at fluence of 1×10^{17} cm^{-2}, where the values of maximum irradiation damage and He concentration are almost equivalent to the peak damage and He ion concentration of ~4.01 dpa and 4.25 at.% of the ultra-fine nano-crystalline $Al_{1.5}CoCrFeNi$ HEA film irradiated at fluence of 5×10^{16} cm^{-2}, respectively. As observed from the HRTEM images, the average size of nano-crystalline with ellipsoid shape (marked by dash line in Fig. 2(b)) in irradiated HEA film is about 6 nm which is in agreement with the calculated grain sizes. Some studies indicate that helium prefers to combine with vacancies to form helium-vacancy complexes (He-V), which block the migration of grain boundary to inhibit grain growth [19,26–27], resulting in that the crystalline size of $Al_{1.5}CoCrFeNi$ HEA film remained stable during irradiation. Moreover, most of the ribbon-like He clusters are preferentially distributed along the GBs in the slightly irradiated damage region of lower than 120 nm, without obvious He clusters in the grains. With the irradiated depth increased to the peak damage region of about 200 nm (as shown in Fig. 2(c)), the agglomerated ribbon-like He clusters were also mainly distributed at the GBs without formation of He bubbles even though the He concentration is up to 8.50 at.%. The abundant three-dimensional network GBs act as defect sinks in the ultra-fine nano-crystalline $Al_{1.5}CoCrFeNi$ HEA films, which can trap helium during irradiation and reduce the rate of helium accumulation within the grains themselves [19,26–28]. The GBs can provide diffusion channels for migration of the He atoms to agglomerate He clusters and then effectively annihilate the irradiation-induced defects in nano-scale materials which can be confirmed by the computational simulation [18,28]. Besides, the structural disordering was induced at the damaged regions by the nano-scale dislocation loops (marked by red arrows in Fig. 2(c)) in the partial grains. It is interesting to note that some grains with limited irradiation damage keep their stability and integrity by suppressing the damage accumulation due to the elimination of irradiated defect at GBs, suggesting that the design of

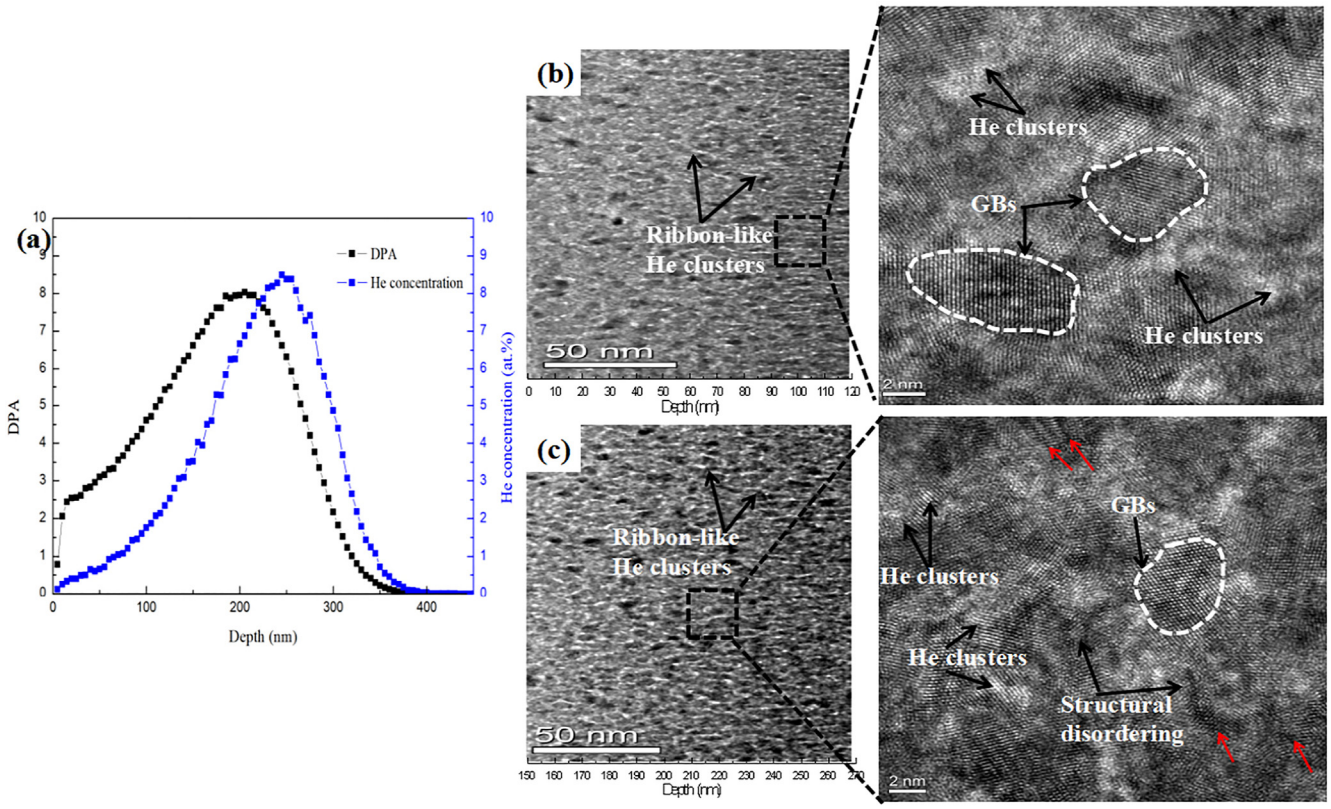

Fig. 2. (a) The displacements per atom (dpa) and He concentration as a function of depth for 60 keV He^+ at fluence of 1×10^{17} cm^{-2}; HRTEM images of a cross-section of ultra-fine nano-crystalline $Al_{1.5}CoCrFeNi$ HEA film irradiated by He^+ at room temperature with fluence of 1×10^{17} cm^{-2}, the high resolution microstructures of HEA film obtained from slightly damaged subsurface layer of ~120 nm width (b) and the damaged region of 150–270 nm in depth from the surface (c), respectively.

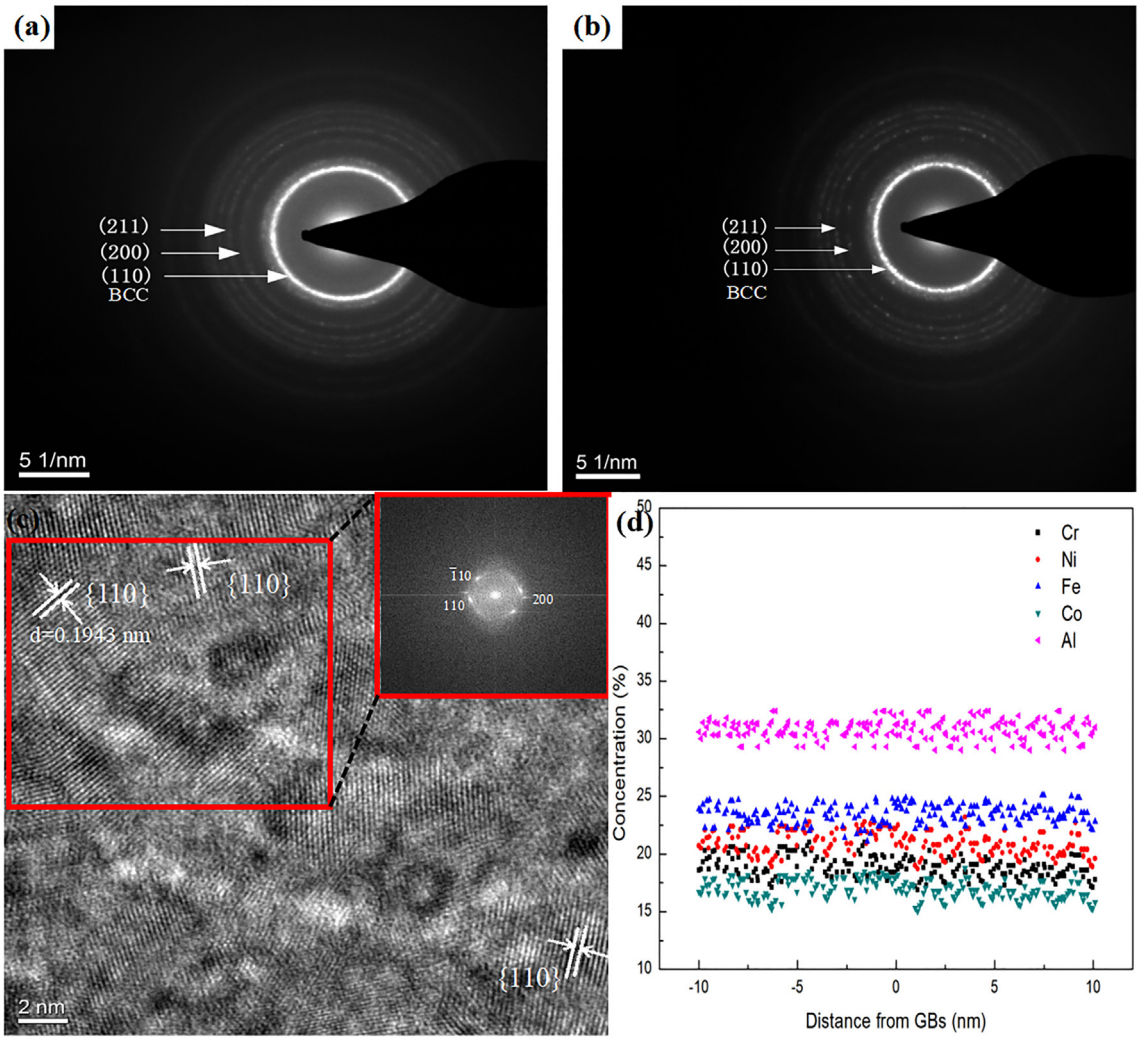

Fig. 3. The SAED patterns of different irradiation damage regions shown in (a) and (b), STEM image (c) and compositional profiles of STEM-EDS (d) of ultra-fine nano-crystalline $Al_{1.5}CoCrFeNi$ HEA films irradiated at fluence of 1×10^{17} cm^{-2}.

ultra-fine nano-crystallines in $Al_{1.5}CoCrFeNi$ HEA films presents enhanced radiation tolerance quality.

Fig. 3 shows the SAED patterns, STEM image and compositional profiles of EDS for the ultra-fine nano-crystalline $Al_{1.5}CoCrFeNi$ HEA film irradiated at fluence of 1×10^{17} cm^{-2}. As shown in Fig. 3(a) and (b), a brightest diffraction ring and another fainter diffraction rings were observed in the SAED patterns which were obtained from different irradiated damage regions, indicating the irradiated HEA film presents polycrystalline BCC phase structure. Besides, there wasn't any extra diffraction rings arising from the BCC matrix. In the inset image of Fig. 3(c), the Fast Fourier Transformation (FFT) transformed from the STEM image of the peak damage region (marked by red squares), in which there wasn't detectable new phases formed except for the BCC phase structure with preferred {1 1 0} planes. Therefore, there wasn't phase decomposition or inherent precipitation in the ultra-fine nano-crystalline $Al_{1.5}CoCrFeNi$ HEA films even under the irradiation damage increased to 8.03 dpa, according to the above analysis results. The new phases nucleation and growth were induced by RIS when the concentration of solute atoms at the sinks exceeds the solubility in the alloy [13–14]. The segregation behavior of composition elements can be characterized by STEM-EDS line-scans. The representative compositional profiles across the GBs were extracted at the peak damage region as shown in Fig. 3(d). The result revealed a slight fluctuation of element concentration in the $Al_{1.5}CoCrFeNi$ HEA films without obvious segregation of the alloy elements near the GBs.

In general, the RIS behavior of major elements, such as Fe, Cr and Ni, at GBs in austenitic stainless steels can be explained by the mechanism of inverse Kirkendall effect (IKE) [29] and solute drag coupled with the diffusional flow of vacancies or interstitials [30], in which the solute enrichment and depletion by the flow of vacancies toward sinks could produce undesirable phases and solute segregation during irradiation. Thus the segregation behavior depends on the flow of vacancies toward defect sinks and diffusion rate of different-size solute atoms, and the mechanisms controlling RIS was also applicable to the HEAs materials [16–18]. However, a dynamic balance of element concentration was characterized near the ultra-fine nano-meter GBs in the irradiated $Al_{1.5}CoCrFeNi$ HEA film, indicating that the phase stability can be controlled by the suppression of RIS level at the GB defect sinks. The introduced He atoms preferentially combine with the vacancies to form He clusters or He-V complexes in the irradiated $Al_{1.5}CoCrFeNi$ HEA films, and finally reducing the vacancy concentration in the grains of HEA films, which contribute to the suppression of the vacancy fluxes toward the defect sink of GBs and subsequent weak RIS behavior in $Al_{1.5}CoCrFeNi$ HEA film according to the mechanism of IKE [29,15]. It worth noting that the composition segregation in coarse-grained $Al_{1.5}CoCrFeNi$ and the phase transformation in $Al_{1.5}CrFeNi$ HEA were both detected due to the irradiation-induced high density vacancy-type defects and voids, respectively [8,31]. The design of three-dimension network GBs in the $Al_{1.5}CoCrFeNi$ HEA film plays an important role in reducing the level of RIS by eliminating the point defects and

facilitating the solute diffusion uniformity and interstitial/vacancy recombination, thus leading to the suppression of solutes enrichment and depletion at the defect sink, which is consistent with the limited RIS in ultra-fine grained 316 austenitic steel after heavy ion irradiation and in the nano-crystalline (1–24 nm grain size) Zr-Hf-Nb alloy after electron irradiation, respectively [20,32]. Lu et al. has studied the unobvious solute segregation in irradiated CoCrFeNiMn HEA bulk materials, in which they attributed the reduced and minimal dislocation RIS to high lattice distortion due to the addition of oversized atoms Mn and Cr that may significantly slow defect diffusion and enhance the vacancy/interstitial recombination resulting in suppressing of the overall vacancy flux to point defect sinks (The atom radius is summarized as follows: $R_{Al} > R_{Mn} > R_{Cr} > R_{Fe} > R_{Co} > R_{Ni}$) [15]. Moreover, the early reported RIS in FeCrNi or FeCoCrNi alloy has shown that the alloy composition plays a significant role in its diffusion and segregation behavior [28,14]. The difference of atomic size induced high lattice strain in multicomponent alloy could produce sluggish diffusion of certain solute atoms. Every lattice site in a multicomponent HEA matrix is occupied by different kinds of atoms. Thus a lattice strain due to the atomic size difference is expected. The calculated maximum difference in the atomic radius in $Al_{1.5}CoCrFeNi$ HEA films is approximate 9.7% based on the equations below [21]:

$$\Delta R_{max} = (R_i - R_a)/R_a \tag{2}$$

$$R_a = \sum_{i=1}^{n} R_i C_i \tag{3}$$

where R_a is the average atomic radius, R_i is atomic radius of component and C_i is the molar percent of component. The maximum calculated misfit ΔR_{max} between the solute atoms in $Al_{1.5}CoCrFeNi$ HEA is about 9.7%, which is close to the 12% limit for solute stability [33]. Chou et al. has pointed out that the larger lattice distortion in $Al_{1.5}CoCrFeNi$ HEA was caused by larger amount of larger atomic size (1.43 Å in radius) of Al into the lattice of smaller atoms (about 1.25 Å in radius for other atoms) [34]. The reduced level of RIS near GBs also results from the elastic strain energy which is associated with misfit atom lattice distortion. The enhanced compositional complexity and high configurational entropy in $Al_{1.5}CoCrFeNi$ HEA films also cause the significant atomic traps and blocks in single-phase multicomponent solid solution owing to the sluggish diffusion [7–8,35–36]. Therefore, the effect of ultra-fine nano-crystalline and high lattice distortion leads to a favorable phase stability by suppressing the level of RIS under He^+ irradiation.

Fig. 4 shows the variation in swelling induced by He clusters as a function of irradiation depth. The swelling values of the ultra-fine nano-crystalline HEA film and coarse-grained bulk HEA irradiated to 1×10^{17} cm^{-2} were calculated from HRTEM images by the equation [37]:

$$S(\%) = \frac{\frac{\pi}{6}\sum_{i=1}^{N} d_i^3}{A \times \delta - \frac{\pi}{6}\sum_{i=1}^{N} d_i^3} \times 100\backslash\% \tag{4}$$

where A is the image area, δ is the sample thickness, d_i is the size of He clusters, N is the number of clusters. For the ultra-fine nano-crystalline HEA film, the swelling is ranging from 0.02% to 1.20% within the irradiation depth, which is significantly lower than the coarse-grained bulk HEA (The swelling is 0.36–3.08%). This is due to the fact that the He clusters mainly distributed at GBs rather than in grains for the ultra-fine nanocrystalline HEA film, as revealed by HRTEM in Fig. 2. The design of ultra-fine nano-crystalline plays an important role in improving swelling resistance by reducing the size of He clusters, which is consistent with the previous research reporting that the grain boundaries act as strong point defect sinks and suppress swelling by reducing the vacancy [38]. However, the introduced He atoms prefer to aggregate with the irradiation-induced vacancies and imperfect lattice in grains for the HEA bulk materials, leading to larger size He bubbles

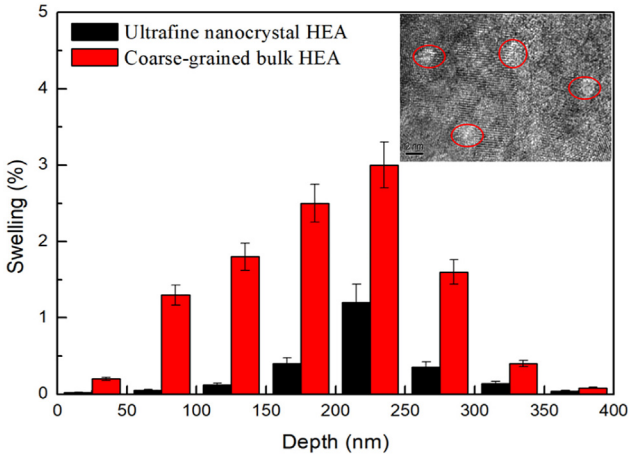

Fig. 4. Irradiation-induced swelling as a function of the depth for ultra-fine nanocrystalline $Al_{1.5}CoCrFeNi$ HEA and coarse-grained bulk HEA irradiated at 1×10^{17} cm^{-2}. The inset HRTEM image shows the micro-structure of coarse-grained $Al_{1.5}CoCrFeNi$ HEA bulk materials irradiated with the fluence of 1×10^{17} cm^{-2}.

(marked by red ellipse) and He-vacancy type nanometer complexes distributed in the coarse-grained bulk $Al_{1.5}CoCrFeNi$ HEA which was irradiated at fluence of 1×10^{17} cm^{-2}, as shown in the inset HRTEM image of Fig. 4. It is well known that the extremely low solubility of helium in metal or alloys can exacerbate precipitation of He into clusters or bubbles at defect sinks, such as vacancies, imperfect lattice and voids, etc [39]. More vacancies and imperfect lattices in the grains of bulk $Al_{1.5}CoCrFeNi$ HEA can be produced by the He^+ bombardment during irradiation, resulting in diverse bubble nucleation and growth behavior. The induced He bubbles and He-vacancy type nanometer complexes in coarse grains of bulk HEA leads to more significant swelling than the HEA film. According to the above results, the ultra-fine nano-crystalline HEA film displays more excellent resistance against swelling than the counterpart of coarse-grained HEA bulk materials.

The relative hardness H/H_0 (H: irradiated hardness, H_0: unirradiated hardness) of the ultra-fine nano-crystalline and coarse-grained $Al_{1.5}CoCrFeNi$ HEA samples as a function of penetration depth were shown in Fig. 5. According to the Depth-H/H_0 curves in Fig. 5(a), the relative hardness H/H_0 in the ion irradiation region of the ultra-fine nano-crystalline $Al_{1.5}CoCrFeNi$ HEA films increased with the He^+ fluence from 1×10^{16} cm^{-2} to 1×10^{17} cm^{-2}. A similar trend in relative hardness H/H_0 was also observed (shown in Fig. 5(b)) in coarse-grained $Al_{1.5}CoCrFeNi$ HEA after irradiation at the same He^+ fluences, but with lower increase rates of H/H_0 than that of ultra-fine nano-crystalline HEA films. When the fluence is ranging from 1×10^{16} cm^{-2} to 3×10^{16} cm^{-2}, only undetectable nano-scale He clusters were introduced in both of ultra-fine nano-crystalline and coarse-grained $Al_{1.5}CoCrFeNi$ HEA. The H/H_0 may be insensitive to the invisible nano-scale He clusters when the fluence less than 3×10^{16} cm^{-2}. The higher increase rate of H/H_0 in irradiated ultra-fine nano-crystalline HEA film can be explained by the Hall-Petch hardening model [40], which indicates that the ultra-fine nano-crystalline was regarded as dominant hardening mechanism in irradiated HEA films. As the fluence further increased from 5×10^{16} cm^{-2} to 1×10^{17} cm^{-2}, except for the Hall-Petch model, the higher of hardening rate can be also interpreted with commonly accepted models proposed by Orowan and Seeger [41]. In these models, the presence of irradiation defects such as He clusters and nano-scale dislocation loops can serve as obstacles to resist the glide of dislocations, which is responsible for the higher hardening rate in the irradiated ultra-fine nano-crystalline HEA films. In order to quantify the contribution of defect cluster on hardening in the ultra-fine nano-crystalline and coarse-grained $Al_{1.5}CoCrFeNi$ HEA, the measured

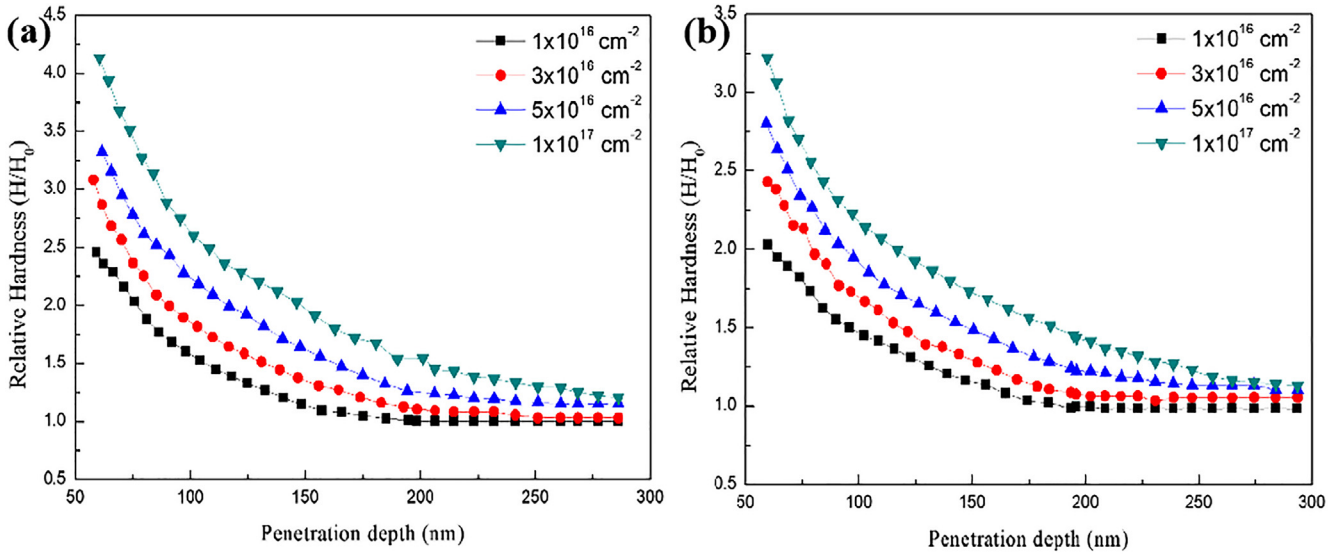

Fig. 5. Variation of relative hardness H/H_0 (H: irradiated hardness, H_0: unirradiated hardness) as a function of penetration depth for ultra-fine nano-crystalline (a) and coarse-grained $Al_{1.5}CoCrFeNi$ HEA (b) irradiated with fluence from 1×10^{16} cm^{-2} to 1×10^{17} cm^{-2}.

increase rate of hardness is compared in the following with the predictions from the well-known dispersed barrier hardening model [42]:

$$\Delta\sigma_y = M\alpha\mu b\sqrt{(Nd)} \quad (5)$$

where $\Delta\sigma_y$ is the yield strength increase, M is Taylor factor (0.36 for equiaxed BCC and FCC metals), α is the barrier strength factor, μ is shear modulus, b is the Burger vector of the gliding dislocation, N is the defect cluster density and d is cluster diameter. The increase of hardening rate in irradiated ultra-fine nano-crystalline $Al_{1.5}CoCrFeNi$ HEA film is more pronounced compared with the coarse-grained HEA at the He^+ fluence ranging from 5×10^{16} cm^{-2} to 1×10^{17} cm^{-2}. The irradiated HEA film had a He cluster density of 1.24×10^{22} m^{-3} –2.5×10^{22} m^{-3} calculated from HRTEM image, whereas large size He bubbles and He-vacancy type nanometer complexes (as shown the inset image of Fig. 4) with slightly lower defect density were both formed in coarse-grained HEA materials. As the explanation in previous paragraph, the introduced helium can exacerbate precipitation of He into clusters and bubbles at defect. Moreover, the previously formed He clusters and bubbles can serve as strong traps for the newly injected He atoms after a short incubation period, resulting in the growth of He bubble, which significantly causes property degradation of structural materials [43]. The mature He bubbles with size of 2–3 nm at the irradiated regions of coarse-grains bulk HEA triggered crystalline embrittlement, which was treated as dominated mechanism in the deterioration of hardening effect for $Al_{1.5}CoCrFeNi$ HEA bulk materials.

4. Conclusion

In summary, the He evolution behavior, radiation tolerance and mechanical behavior in ultra-fine nano-crystalline $Al_{1.5}CoCrFeNi$ HEA films were investigated in this study. The results revealed that the He clusters preferentially distributed along the nano-GBs rather than in grains due to the defect sinks effects. There wasn't observable He bubbles formed in the films even though the peak He concentration is up to 8.50 at.% at the fluence of 1×10^{17} cm^{-2}. Some grains with limited irradiation damage keep their stability and integrity by suppressing damage accumulation, exhibiting excellent radiation tolerance for the HEA film. The effect of ultra-fine nano-crystalline and high lattice distortion leads to a favorable phase stability in irradiated $Al_{1.5}CoCrFeNi$ HEA films by suppressing the level of RIS. Moreover, the ultra-fine nano-crystalline structure in HEA films plays an important role in improving swelling resistance by reducing the size of He clusters, displaying excellent swelling resistance than that of the irradiated coarse-grained HEA bulk materials. The different He evolution behavior and irradiated defects between the ultra-fine nano-crystalline HEA films and coarse-grained HEA bulk materials are responsible for the hardening rate. Therefore, the ultra-fine nano-crystalline HEA materials may be one of good candidates for the future advanced nuclear reactor's structural materials.

CRediT authorship contribution statement

Guo Pu: Conceptualization, Data curation, Formal analysis, Writing - original draft. **Liwei Lin:** Resources, Software. **Ran Ang:** Visualization. **Kun Zhang:** Funding acquisition. **Bo Liu:** Investigation, Methodology. **Bin Liu:** Supervision. **Tao Peng:** Project administration. **Shifeng Liu:** Validation. **Qiran Li:** Writing - review & editing.

Declaration of Competing Interest

The authors declare that they have no known competing financial interests or personal relationships that could have appeared to influence the work reported in this paper.

Acknowledgments

This work was supported by the Shenzhen Science and Technology Research and Development Fund Project, China (Project Nos. JCYJ20180302145708405 and JCYJ2017041316410226), and the National Natural Science Foundation of China, China (Grant No. 11605116, 51771126). The author Kun Zhang is grateful to the Fundamental Research Funds for the central Universities for its financial supports.

References

[1] S.J. Zinkle, J.T. Busby, Structural materials for fission & fusion energy, Mater. Today 12 (2009) 12–19.
[2] J.W. Yeh, S.K. Chen, S.J. Lin, J.Y. Gan, Nanostructured high-entropy alloys with multiple principal elements: novel alloy design concepts and outcomes, Adv. Eng. Mater. 6 (2004) 299–303.
[3] M.C. Troparevsky, J.R. Morris, M. Daene, Beyond atomic size and hume-rolues: understanding and predicting high entropy alloys, JOM 67 (2015) 2350–2363.
[4] B. Gludovatz, A. Hohenwarter, D. Catoor, E.H. Chang, A fracture resistant high entropy alloy for cryogenic application, Science 345 (2014) 1153–1158.
[5] F. Otto, A. Dlouhy, C. Somsen, H. Bei, G. Eggeler, The influence of temperature and

microstructure on the tensile properties of a CoCrFeMnNi high entropy alloy, Acta Mater. 61 (2013) 5743–5755.
[6] S.Q. Xia, X. Yang, T.F. Yang, S. Liu, Y. Zhang, Irradiation resistance in AlxCoCrFeNi high entropy alloys, JOM 67 (2015) 2340–2344.
[7] S.Q. Xia, M.C. Gao, T. Yang, P.K. Liaw, Phase stability and microstructure of high entropy alloys ion irradiated to high doses, J. Nucl. Mater. 480 (2016) 100–108.
[8] T.F. Yang, S.Q. Xia, S. Liu, Y. Fang, Y. Zhang, J. Xue, S. Yan, Y. Wang, Precipitation behavior of AlxCoCrFeNi high entropy alloys under ion irradiation, Sci. Rep. 6 (2016) 32146.
[9] C. Lu, L. Niu, N. Chen, K. Jin, T. Yang, P. Xiu, Y. Zhang, F. Gao, H. Bei, S. Shi, M.R. He, I.M. Robertson, W.J. Weber, L. Wang, Enhancing irradiation tolerance by controlling defect mobility and migration pathways in multicomponent single phase alloys, Nat. Commun. 7 (2016) 13564.
[10] S. Zhao, Y. Osetsky, Y. Zhang, Preferential diffusion in concentrated solid solution alloys: NiFe NiCo and NiCoCr, Acta Mater. 128 (2017) 391–399.
[11] D. Chen, Y. Tong, H. Li, J. Wang, Y.L. Zhao, A. Hu, J.J. Kai, Helium accumulation and bubble formation in FeCoCrNi alloy under high fluence He^+ implantation, J. Nucl. Mater. 501 (2018) 208–216.
[12] D. Chen, Y. Tong, J. Wang, B. Han, Y.L. Zhao, Microstructural response of He^+ irradiated $FeCoNiCrTi_{0.2}$ high entropy alloy, J. Nucl. Mater. 510 (2018) 187–192.
[13] B. Kombaiah, K. Jin, H. Bei, P.D. Edmondson, Y. Zhang, Phase stability of single phase $Al_{0.12}$CrNiFeCo high entropy alloy upon irradiation, Mater. Des. 160 (2018) 1208–1216.
[14] M.-R. He, S. Wang, S. Shi, K. Jin, H. Bei, K. Yasuda, S. Matsumura, K. Higashida, I.M. Robertson, Mechanisms of radiation-induced segregation in CrFeCoNi-based single-phase concentrated solid solution alloys, Acta Mater. 126 (2017) 182–193.
[15] C. Lu, T. Yang, K. Jin, N. Gao, P. Xiu, Y. Zhang, F. Gao, H. Bei, W.J. Weber, K. Sun, Y. Dong, L. Wang, Radiation induced segregation on defect clusters in single phase concentrated solid solution alloys, Acta Mater. 127 (2017) 98–107.
[16] S. Roy, J. Ghatak, B.N. Dev, Ion irradiation induced evolution of nanostructure in a graded multi-trilayer system, App. Sur. Sci. 258 (2012).
[17] Ch.M. Barr, J.E. Nathaniel II, K.A. Unocic, J.P. Liu, Y. Zhang, Y. Wang, Mitra, L. Taheri, Exploring radiation induced segregation mechanism at grain boundaries in equiatomic CoCrFeNiMn high entropy alloy under heavy ion irradiation, Scr. Mater. 156 (2018) 80–84.
[18] Z. Jiao, G.S. Was, Novel features of radiation induced segregation and radiation induced precipitation in austenitic stainless steels, Acta Mater. 59 (2011) 1220–1238.
[19] N. Nita, R. Schaeublin, M. Victoria, Impact of irradiation on the microstructure of nanocrystalline materials, J. Nucl. Mater. 329–333 (2004) 953–957.
[20] A. Etienne, B. Radiguet, N.J. Cunningham, Comparison of radiation induced segregation in ultrafine-grained and conventional 316 austenitic stainless steels, Ultramicroscopy 111 (2011) 659–663.
[21] N.A.P. Kiran Kumar, C. Li, K.J. Leonard, H. Bei, S.J. Zinkle, Micro-structural stability and mechanical behavior of FeNiMnCr high entropy alloy under ion irradiation, Acta Mater. 113 (2016) 230–244.
[22] G. Odette, M. Alinger, B. Wirth, Recent developments in irradiation-resistant steels, Annu. Rev. Mater. Res. 38 (2008) 471–503.
[23] W.J. Weber, Y.W. Zhang, Predicting damage production in monoatomic and multi-elemental targets using stopping and range of ions in matter code: Challenges and recommendationsOn the use of SRIM for computing radiation damage exposure, Solid State Mater. Sci. 23 (2019) 100757.
[24] W.R. Wang, W.L. Wang, S.C. Wang, Y.C. Tsai, C.H. Lai, J.W. Yeha, Effects of Al addition on the microstructure and mechanical property of AlxCoCrFeNi high entropy alloys, Intermetallics 26 (2012) 44–51.
[25] Y. Wang, H. Li, L. Ji, F. Zhao, Q. Kong, Y. Wang, X. Liu, Microstructure, mechanical and tribological properties of graphite-like amorphous carbon films prepared by unbalanced magnetron sputtering, Surf. Coatings Technol. 205 (2011) 3058–3065.
[26] C. Fan, Z. Shang, T. Niu, J. Li, H. Wang, X. Zhang, Dual Beam In Situ Radiation Studies of Nanocrystalline Cu, Mater. 12 (2019) 2721.
[27] G.M. Cheng, W.Z. Xu, Y.Q. Wang, A. Misra, Y.T. Zhu, Grain size effect on radiation tolerance of nanocrystalline Mo, Scr Mater. 123 (2016) 90–94.
[28] Y.F. Zh, P.C. Millett, M. Tonks, L.Zh. Zh, B. Biner, Molecular dynamics simulations of He bubble nucleation at grain boundaries, J. Phys.: Condense. Matter. 24 (2012) 305005 (12pp).
[29] T.R. Allen, J.T. Busby, G.S. Was, E.A. Kenik, On the mechanism of radiation-induced segregation in austenitic Fe-Cr-Ni alloys, J. Nucl. Mater. 255 (1998) 44–58.
[30] G.S. Was, J.P. Wharry, B. Frisbie, B.D. Wirth, Assessment of radiation-induced segregation mechanism in austenitic and ferritic - martensitic alloys, J. Nucl. Mater. 411 (2011) 41–50.
[31] S. Sun, et al., Segregation of $Al_{1.5}$CrFeNi high entropy alloy induced by vacancy-type defects, Scr. Mater. 161 (2019) 40–43.
[32] T. Nagase, S. Anada, P.D. Rack, J.H. Noh, H. Yasuda, MeV electron irradiation-induced structural change in the bcc phase of Zr-Hf-Nb alloy with an approximately equiatomic ratio, Intermetallics. 38 (2013) 70–79.
[33] A. Li, X. Zhang, Thermodynamic analysis of the simple microstructure of AlCrFeNiCu high entropy alloy with multi-principal elements, Acta Metall. Sin. Engl. Lett. 22 (2009) 219–224.
[34] H.P. Chou, Y.S. Chang, S.K. Chen, J.W. Yeh, Microstructure, thermophysical and electrical properties in AlxCoCrFeNi ($0 \le x \le 2$) high-entropy alloys, Mate. Sci. Eng. B. 163 (2009) 184–189.
[35] M.H. Tsai, C.W. Wang, C.W. Tsai, W.J. Shen, J.W. Yeh, J.Y. Gan, Thermal stability and performance of NbSiTaTiZr high-entropy alloy barrier for copper metallization, J. Electrochem. Soc. 158 (2011) H1161.
[36] S.Y. Chang, C.E. Li, J.W. Yeh, Structural and thermodynamic factors of suppressed interdiffusion kinetics in multi-component high-entropy materials, Sci. Rep. 4 (2014) 4162.
[37] M.B. Toloczko, F.A. Garner, Ion-induced swelling of ODS ferritic alloy MA957 tubing to 500dpa, J. Nucl. Mater. 450 (2014) 323–333.
[38] G. Ayrault, Cavity formation during single- and dual-ion irradiation in a 9Cr-1Mo ferritic alloy, J. Nucl. Mater. 114 (1983) 34–40.
[39] W.D. Nix, H. Gao, Indentation size effects in crystalline materials: a law for strain gradient plasticity, J. Mech. Phys. Solids 46 (1998) 411–425.
[40] E. Martínez, J. Romero, A. Lousa, J. Esteve, Nanoindentation stress - strain curves as a method for thin-film complete mechanical characterization: application to nanometric CrN/Cr multilayer coatings, Appl. Phys. A (Mater. Sci. Process.) 77 (2003) 419–427.
[41] E. Orowan, Internal Stresses in Metals and Alloys, Institute of Metals, London, 1948, p. 451.
[42] A. Seeger, Proceedings of the 2nd International Conference on Peaceful Uses of Atomic Energy Geneva, International Atomic Energy Agency, Vienna, Austria, 1985, p. 250.
[43] H. Ullmaier, The influence of helium on the bulk properties of fusion reactor structural materials, Nucl. Fusion. 24 (1984) 1039–1083.